NUMERICALLY FOCUSED OPTICAL COHERENCE MICROSCOPY WITH STRUCTURED ILLUMINATION APERTURE

A.A. Grebenyuk [1, 2, 3], V.P. Ryabukho [1, 2]
[1] Saratov State University, Saratov, Russia,
[2] Institute of Precision Mechanics and Control of the Russian Academy of Sciences, Saratov, Russia,
[3] Currently with the Christian Doppler Laboratory OPTRAMED,
Center for Medical Physics and Biomedical Engineering, Medical University of Vienna, Vienna, Austria

Abstract

In optical coherence microscopy (OCM) with a given numerical aperture (*NA*) of the objectives the transverse resolution can be increased by increasing the numerical aperture of illumination (*NAi*). However, this may also lead to attenuation of the signal with defocus preventing the effective numerically focused 3D imaging of the required sample volume. This paper presents an approach to structuring the illumination aperture, which allows combining the advantages of increased transverse resolution (peculiar to high *NAi*) with small attenuation of the signal with defocus (peculiar to low *NAi*) for high-resolution numerically focused 3D imaging in OCM.

Keywords: optical coherence microscopy, optical coherence tomography, numerical focusing, structured illumination, superresolution, image reconstruction techniques.

Citation: Grebenyuk AA, Ryabukho VP. Numerically focused optical coherence microscopy with structured illumination aperture. Computer Optics 2018; 42(2): 248-253. DOI: 10.18287/2412-6179-2018-42-2-248-253.

Acknowledgements: This work has been supported in part by Russian Presidential grant NSh-7898.2016.2.

Introduction

One of the major problems in Fourier domain (FD) optical coherence tomography/microscopy (OCT/OCM) is the trade-off between either high transverse resolution (achieved using objectives with high numerical apertures *NA*) or large depth of field (achieved using objectives with low *NA*). The probably most effective solution of this problem consists in numerical focusing of the recorded OCM signal, which allows extending the region of high transverse resolution in the acquired 3D image beyond the optical focus depth just by numerical processing, e.g. [1 – 4]. This approach thus allows utilization of objectives with relatively high *NA* and achievement of high transverse resolution without compromising the depth of field.

Another factor affecting the transverse resolution in both scanning confocal and full-field (FF) OCM is the numerical aperture of illumination *NAi* [5, 6]. However, increasing the *NAi* for higher transverse resolution may also lead to attenuation of the signal with defocus in spite of the application of a specific numerical focusing procedure, that may pose a problem for effective numerically focused imaging of the required sample volume [4, 7].

Recently we have shown that this problem can be overcome in Linnik-type FD OCM in both the full-field and scanning confocal modalities by organizing a special structure of the illumination aperture function and applying specific numerical focusing [8]. This paper presents a more detailed description of this approach and analysis of its properties. The basic idea is to use the well-known Linnik interferometer with an illumination aperture comprised of a set of small illumination spots, each resulting in a certain illumination direction over the sample, (instead of circular or annular illumination apertures) in combination with a specific numerical processing [4, 7] for numerically focused 3D FD OCM imaging. To provide better coverage of a sample's transverse spatial spectrum and reduce overlapping of transverse spatial spectra of the individual signals, corresponding to different illumination directions, these illumination spots should be maximally remote from each other and close to the physical aperture borders. This approach is suited to FF OCM, which is very promising for numerically focused 3D OCM imaging due to the possibility of parallel data acquisition in the transverse direction, but can also be applied in the case of scanning confocal OCM, as will be discussed below.

It should be noted, that the principle of using off-axis illumination from several directions in order to improve the transverse resolution has been used in different kinds of interference microscopes with sequential or simultaneous use of the different illumination directions, e.g. [9 – 13]. The realization of this principle that we propose is particularly suitable for numerically focused FF FD OCM imaging and allows for parallelization to certain extent of the detection of parts of the OCM signal corresponding to different illumination directions.

1. Principle of numerically focused OCM with structured illumination aperture

Fig. 1 presents an optical scheme of a Linnik-type OCM with an example of a special illumination system for creating a structured illumination aperture (in the point-dash box). The imaging part of this scheme is a general imaging part of a Linnik-type OCM, which with different illumination systems can produce different kinds of time domain (TD) and FD OCM imaging [3, 4, 14 – 16].

A Linnik-type OCM can be used in different modes depending on the type of illumination: spatially incoherent illumination over the objectives' apertures corresponds to the FF mode, while spatially coherent illumina-

tion over the objectives' apertures corresponds to the scanning confocal mode [16]. This means that when organizing an illumination aperture from several illumination spots for a FF OCM, the illumination fields in these spots should be mutually incoherent. In particular, this means, that in the FF case the intensity of the illumination field is to be approximately uniform across the field of view, without a fringe pattern, peculiar to straightforward implementation of conventional structured illumination in interference microscopy [12, 13].

Such illumination can be realized in many ways, e.g. by splitting the illumination field from a single source for creating several illumination points and creating sufficient optical delays along with the splitting in order to make the illumination points mutually incoherent (e.g. as shown in Fig. 1).

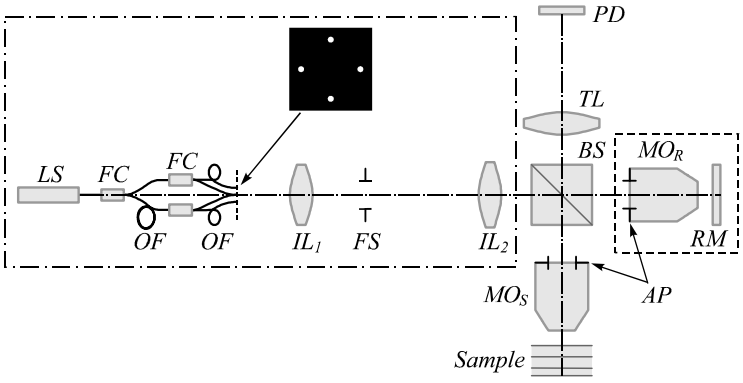

Fig. 1. Optical scheme of a FF swept-source OCM based on a Linnik-type interference microscope with an illumination system for creating a structured illumination aperture. MO_S and MO_R – objectives in the sample and reference arms, RM – reference mirror, AP – objectives' aperture planes in the back focal planes of the respective objectives, TL – tube lens, BS – beam splitter, PD – matrix photodetector, IL_1, IL_2 – lenses of the illumination system, FS – field stop of the illumination system, OF – optical fibers, FC – fiber couplers, LS – swept laser source. The lengths of the fibers are selected in such a way, that the illumination points, imaged onto the aperture planes, can be considered mutually incoherent

For general analysis, applicable to both FF and scanning confocal OCM modes one can make use of the similarity between the coherence signals of FF and confocal OCM (provided that the reference mirror is in the focus of the respective objective) [4, 7] by using the concept of the illumination aperture function [4, 8]. In the case of FF Linnik-type OCM the illumination aperture function can be defined as [4]

$$A_i(\omega;x_0,y_0)=I_0(\omega;x_0,y_0)A^*(\omega;-x_0,-y_0)\times \\ \times r_R^*\left(\omega;-k\frac{x_0}{f'},-k\frac{y_0}{f'}\right), \quad (1)$$

where $\omega=2\pi\nu$ is the circular temporal frequency, ν is the linear temporal frequency, I_0 is the spectral density of the illumination field immediately after passing the objective's aperture, A is the objectives' aperture function, r_R is the amplitude reflection coefficient of the reference mirror, $k=\omega/c$ is the wavenumber, c is the light speed in vacuum, f' is the back focal distance of the objectives. In the case of confocal OCM the complex amplitude distribution of the illumination field immediately after passing the objective's aperture can be termed the illumination aperture function [8].

FD OCM allows acquiring quasimonochromatic coherence signals with different central temporal frequencies, which can approximately be considered proportional to the mutual spectral density of the sample and reference arms' fields $\Gamma(\omega;x,y)$ at the central frequency of the respective quasimonochromatic signal. The reconstruction of these coherence signals can be done in different ways e.g. by phase-shifting or by Fourier filtration in the temporal spectrum domain (e.g. after shifting as whole the reference objective together with the reference mirror along the optical axis [4]). Numerical refocusing can be applied to these quasimonochromatic coherence signals in various ways. This paper employs the numerical processing algorithms (which include numerical focusing) of [4, 7], which can take into account an arbitrary shape of the illumination aperture function.

2. Signal properties in numerically focused OCM with structured illumination aperture

Figs. 2–5 present the results of numerical simulation based on the theory presented in [4] in the case of $NA=0.2$. For numerical simulation of the mutual spectral density before numerical focusing the following equations have been used [4]:

$$\Gamma(\omega;x,y)=(2\pi)^{-2}\iint\tilde{\Gamma}(\omega;k_x,k_y)\times \\ \times\exp[i(k_xx+k_yy)]\mathrm{d}k_x\mathrm{d}k_y, \quad (2)$$

$$\tilde{\Gamma}(\omega;k_x,k_y)\approx\mu_0(\omega)M^2\left[\prod_{j=1}^{N}t_{j-1,j}(\omega)t_{j,j-1}(\omega)\right]\times \\ \times\tilde{r}_S(\omega;-Mk_x,-Mk_y)\Xi(\omega;k_x,k_y), \quad (3)$$

$$\mu_0(\omega)=\lambda^{-4}f'^{-2}f_L'^{-2}, \quad (4)$$

$$\Xi(\omega;k_x,k_y)=\iint\mathrm{d}x_S\mathrm{d}y_S\exp[-iM(k_xx_S+k_yy_S)]\times \\ \times\iint A(\omega;x_3,y_3)\exp\left[ik\sum_{j=0}^{N}\Delta z_j\sqrt{n_j^2-(x_3^2+y_3^2)/f'^2}\right]\times \\ \times\exp[-i(k/f')(x_3x_S+y_3y_S)]\mathrm{d}x_3\mathrm{d}y_3\times \\ \times\iint A_i(\omega;x_0,y_0)\exp\left\{ik\left[(z_S-2z_R+|f|)\times\right.\right. \\ \left.\left.\times\sqrt{n_0^2-(x_0^2+y_0^2)/f'^2}+\sum_{j=1}^{N}\Delta z_j\sqrt{n_j^2-(x_0^2+y_0^2)/f'^2}\right]\right\}\times \\ \times\exp[-i(k/f')(x_0x_S+y_0y_S)]\mathrm{d}x_0\mathrm{d}y_0, \quad (5)$$

where the tilde sign denotes the transverse spatial spectrum of the respective function, k_x and k_y are circular transverse spatial frequencies, r_S is the amplitude reflection coefficient of the imaged interface in the sample, M is the absolute value of transverse magnification; $t_{j\text{-}1,j}$ are

the transmission coefficients of the sample interfaces; n_j and Δz_j for $j \geq 1$ are the refractive indices and thicknesses of the sample layers; N is the number of sample layers above the imaged interface; λ is the wavelength in vacuum, f_L' is the back focal distance of the tube lens, z_S is the distance from the front principal plane of MO_S to the sample surface, z_R is the distance from the front principal plane of MO_R to the reference mirror, f is the front focal distance of the objectives, n_0 is the refractive index of immersion, $\Delta z_0 = z_S - |f|$, the integrals in (2) – (5) have infinite integration limits. In numerical simulation z_R is assumed to be equal to $|f|$.

Figs. 2 – 5 present the results of numerical simulation of imaging a single scatterer in air by using $N = 0$ (no layered structure in the sample), $n_0 = 1$, $r_S(\omega; x_S, y_S) \sim \delta(x_S)\delta(y_S)$. All the figures except for 2*a* present the results after the application in each case of a specific numerical processing procedure (including numerical focusing) according to [4]. Similar results can be obtained in the confocal case due to the similarity of the equations for the coherence signal [7]. This simple case of imaging a single scatterer in air is selected to provide clear conclusions on the imaging properties; however in general the approaches of [4, 7] provide the possibility of numerical focusing in the case of imaging in depth of a layered sample.

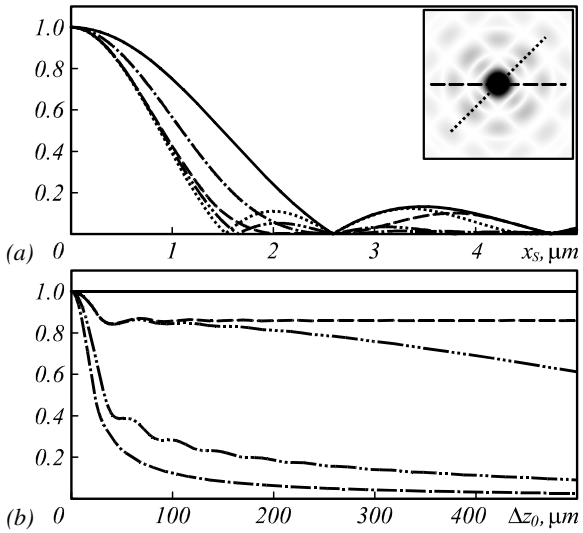

Fig. 2. (a) dependence of $|\Gamma_{PSF}(\omega; x_S, 0)|$ on x_S (except for the point line, which corresponds to $|\Gamma_{PSF}(\omega; x_S/\sqrt{2}, x_S/\sqrt{2})|$ in the case of structured illumination as explained in the inset) in the absence of defocus; (b) attenuation of the absolute value of numerically focused Γ_{PSF} at $x_S = 0$, $y_S = 0$ with defocus Δz_0; (in (a) the graphs for structured illumination with NAir = 0.002 are not shown as they are very similar to the respective graphs for structured illumination with NAir→0). In all graphs the absolute values of Γ_{PSF} are normalized for each illumination aperture, so that they have a unity value at $x_S = 0$, $y_S = 0$ in the absence of defocus (at $\Delta z_0 = 0$). (The contrast in the inset is inverted - higher values of $|\Gamma_{PSF}|$ correspond to lower gray levels)

The signal from a single scatterer is essentially a transverse impulse response (transverse point spread function, PSF). Scaled to the sample space ($x_S = x/M$, $y_S = y/M$) it can be denoted as $\Gamma_{PSF}(\omega; x_S, y_S)$ in the case of a numerically focused mutual spectral density signal (monochromatic coherence signal) and $\Gamma_{PSF}^{(t)}(x_S, y_S)$ in the case of a total signal, comprised of multiple numerically focused monochromatic signals according to the FD OCT/OCM principle. Figs. 2 and 3($a-c$) correspond to monochromatic signals with $\nu = 3.53\times10^{14}$ Hz (which corresponds to $\lambda \approx 850$ nm); Figs. 3($d-f$) and Figs. 4 – 5 correspond to total numerically focused signals (after a combination of 512 monochromatic signals with a total central temporal frequency $\nu_0 = 3.53\times10^{14}$ Hz and a total temporal spectrum width $\Delta\nu = 4.15\times10^{13}$ Hz, which corresponds to $\Delta\lambda \approx 100$ nm).

Fig. 2 presents a comparison of the basic properties of Γ_{PSF} in the cases of OCM with different types of illumination aperture after the application of a specific numerical focusing procedure in each case. The continuous line corresponds to point illumination aperture ($NAi \to 0$) centered on the optical axis (which corresponds to plane-wave illumination over the sample); the point-dash line corresponds to uniform circular illumination aperture with $NAi = NA$ (illumination field fills completely the apertures of the objectives); the two points – dash line corresponds to annular illumination with inner and outer radii corresponding to $NAi_1 = 0.194$ and $NAi_2 = 0.198$ respectively; the three points - dash line corresponds to a structured illumination aperture comprised of four small illumination circles with centers shifted from the optical axis at $NAic = 0.196$ and radii corresponding to $NAir = 0.002$ (in the FF case this means partially spatially coherent illumination from each of the illumination directions); the dash and point lines correspond to a structured illumination aperture comprised of four infinitely small illumination points ($NAir \to 0$, which corresponds to spatially coherent illumination from each of the illumination directions) with centers shifted from the optical axis at $NAic = 0.196$ (this latter case corresponds to the illumination system in Fig. 1). As has been noted above, it is desirable to place the illumination spots as close as possible to the physical aperture borders, however in practice even in the case of $NAir \to 0$, $NAic$ has to be somewhat smaller than NA, especially when using displacement of the reference objective with the mirror.

As can be seen from Fig. 2*a*, the circular, annular and structured illumination apertures provide comparable transverse resolution, significantly higher, than in the case of plane-wave illumination along the optical axis. The full width at half maximum (FWHM) of Γ_{PSF} in the case of structured illumination with $NAir \to 0$ along the dash and point lines is approximately 1.8 and 1.76 μm, while in the case of plane-wave illumination (continuous line) FWHM is approximately 3 μm. The structured and annular illumination apertures provide narrower Γ_{PSF} than the circular one, however at the cost of increased sidelobes. In addition, the structured illumination leads to a not circularly symmetric Γ_{PSF} shape, which can be clearly seen from comparison of the dash line and point line, corresponding to the Γ_{PSF} shape along the different transverse directions.

On the other hand, both circular and annular illumination apertures lead to significant signal attenuation with defocus, in spite of the application of a specific numerical refocusing technique in each case. This is a consequence of the longitudinal coherence gate related to the angular spectrum of the optical field (not the temporal spectrum width) and therefore is present even in the mutual spectral density. This effect can be tolerable in certain circumstances (as discussed in [4]), especially in the case of an annular illumination aperture. However, in general this attenuation may pose a problem for numerically focused 3D imaging. Structured illumination provides much less attenuation with defocus. Small but finite size of the illumination spots of structured illumination (in the FF case corresponding to partially spatially coherent illumination from each of the illumination directions) can be used for introducing a small attenuation, not significant for the imaged region, but leading to suppression of coherent noise originating from the regions far from the focus.

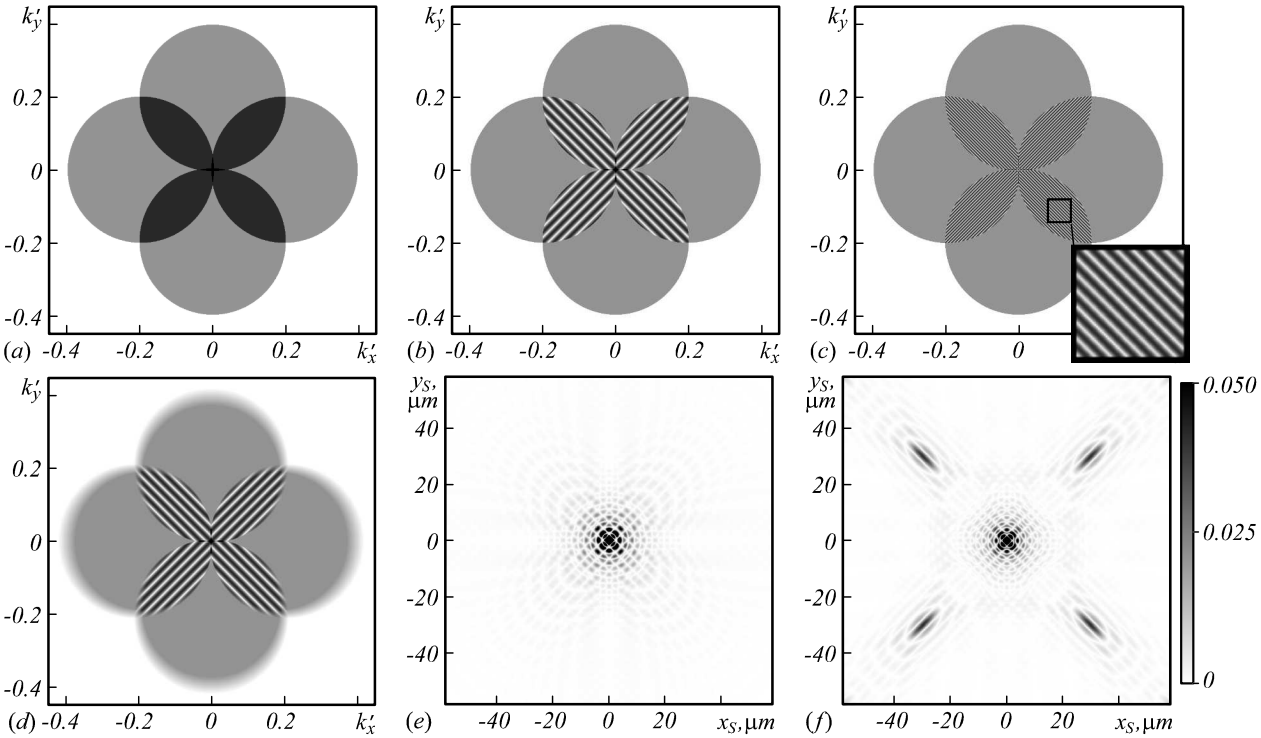

Fig. 3. (a – c) Absolute values of the spatial spectra of Γ_{PSF} at defocus of 0, 150 and 500 μm; (d) absolute values of the spatial spectrum of $\Gamma^{(t)}_{PSF}$ at a defocus of 150 μm; (e) and (f) $|\Gamma^{(t)}_{PSF}|$ at defocus values of 0 and 150 μm (the gray level bar on the right of (f) is applicable to both (e) and (f); in this grey level bar unity corresponds to $|\Gamma^{(t)}_{PSF}(0,0)|$ in the absence of defocus). The contrast in all images is inverted – higher values correspond to lower gray levels

Figs. 3 – 5 present a more detailed analysis of the signal properties in the case of structured illumination with $NAic = 0.196$, $NAir \to 0$ with four illumination spots (Figs. 3 – 4) and three illumination spots (Fig. 5). In Figs. 3 and 5 $k'_x = Mk_x / k_0$ and $k'_y = Mk_y / k_0$ are the normalized circular transverse spatial frequencies [4] for the central temporal frequency ν_0.

The spatial spectra in Fig. 3 ($a - d$) are comprised of four circles, each corresponding to a certain illumination direction (illumination spot of the structured illumination aperture). As a benefit of the Linnik-type arrangement, which can work even with spatially low-coherent illumination, these circles are properly located (no need to artificially shift them with respect to each other). However this has also a negative effect: with defocus each of these circles in the spatial spectrum becomes phase modulated and these phase modulations are not matched in the overlapping regions. This leads to the appearance of fringe structures in the total spatial spectrum in the overlapping regions with frequency the higher, the larger is the defocus value.

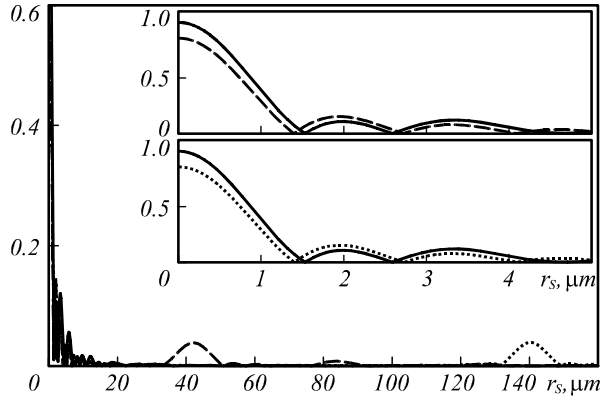

Fig. 4. $|\Gamma^{(t)}_{PSF}(r_S/\sqrt{2}, r_S/\sqrt{2})|$ (at 45 degrees to the x_S axis) at different defocus values Δz_0 (continuous line corresponds to $\Delta z_0 = 0$ μm, dash line corresponds to $\Delta z_0 = 150$ μm, point line corresponds to $\Delta z_0 = 500$ μm)

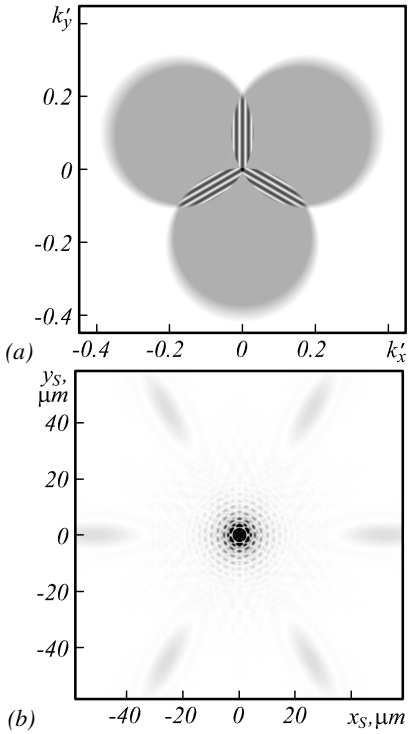

Fig. 5. (a) and (b) numerical simulation results for the case of structured illumination with three illumination spots with other parameters similar to Fig. 3d and f. The contrast in all images is inverted – higher values correspond to lower gray levels

These fringe structures in the spatial spectrum lead to appearance of artifacts in the PSF in the directions, perpendicular to the fringes (Fig. 3*e–f* and Fig. 4). The larger is the defocus value, the higher is the frequency of the fringe structures in the spatial spectrum and hence the further are the artifact sidelobes from the main peak. This explains the small decrease in the PSF magnitude with defocus when using the structured illumination aperture even in the case of $NAir \rightarrow 0$ in Fig. 2*b* as a result of some leakage of energy from the main peak into the artifacts.

For practical application these artifacts can often be neglected. They can also be decreased in different ways by modifying (and hence complicating) the optical scheme. One of the simplest approaches to the artifact suppression is the reduction in the number of illumination directions used simultaneously, which leads to decrease in the size of the overlapping areas in the spatial spectrum and hence decrease of the artifacts magnitude (Fig. 5). However this also means a decrease in the PSF circular symmetry or requires several recordings with different sets of illumination directions, which can be combined numerically providing a bigger total number of illumination directions with decreased artifacts, although at the cost of decreased imaging speed. Therefore the number of illumination directions is to be chosen depending on the particular imaging requirements.

Conclusions

In conclusion, we proposed an approach to FD OCM imaging, combining a Linnik-type OCM with structured illumination aperture with special numerical processing proposed in [4, 7] (which includes numerical focusing taking into account the shape of the illumination aperture function). This approach allows combining the advantages of increased transverse resolution (peculiar to high *NAi*) with small attenuation of the signal with defocus (peculiar to low *NAi*) for high-resolution numerically focused 3D imaging in OCM. It is applicable to both FF and scanning confocal OCM systems and can find applications in many areas, where high-resolution high-speed numerically focused 3D OCM imaging is required.

Finally, it can be pointed out that in OCM (both FF and scanning confocal) the increased transverse resolution (in comparison with the plane-wave illumination) can be achieved by using circular or annular illumination apertures (the latter can be considered as a limiting case of structured illumination with an infinite number of illumination directions), which provide more circularly symmetric transverse PSF, than the structured illumination. The main advantage of using the structured illumination in OCM consists in the combination of the increased transverse resolution effect with the possibility of effective numerical focusing for relatively high-speed high-resolution 3D imaging.

References

[1] Ralston TS, Marks DL, Carney PS, Boppart SA. Interferometric synthetic aperture microscopy. Nature Physics 2007; 3: 129-134. DOI: 10.1038/nphys514.

[2] Hillmann D, Lührs C, Bonin T, Koch P, Hüttmann G. Holoscopy-holographic optical coherence tomography. Opt Lett 2011; 36(13): 2390-2392. DOI: 10.1364/OL.36.002390.

[3] Kumar A, Drexler W, Leitgeb RA. Numerical focusing methods for full field OCT: a comparison based on a common signal model. Opt Express 2014; 22(13): 16061-16078. DOI: 10.1364/OE.22.016061.

[4] Grebenyuk A, Federici A, Ryabukho V, Dubois A. Numerically focused full-field swept-source optical coherence microscopy with low spatial coherence illumination. Appl Opt 2014; 53(8): 1697-1708. DOI: 10.1364/AO.53.001697.

[5] Villiger M, Pache C, Lasser T. Dark-field optical coherence microscopy. Opt Lett 2010; 35(20): 3489-3491. DOI: 10.1364/OL.35.003489.

[6] Grebenyuk AA, Ryabukho VP. Theory of imaging and coherence effects in full-field optical coherence microscopy. In Book: Dubois A, ed. Handbook of full-field optical coherence microscopy. Singapore: Pan Stanford Publishing; 2016. Chap 2: 53-89.

[7] Grebenyuk AA, Ryabukho VP. Numerical reconstruction of 3D image in Fourier domain confocal optical coherence microscopy. Proceedings of the International Conference on Advanced Laser Technologies 2012. DOI: 10.12684/alt.1.60.

[8] Grebenyuk AA, Ryabukho VP. Illumination structure and three-dimensional imaging properties in optical coherence microscopy [In Russian]. Proceedings of the International School-Conference for Young Scientists and Specialists "Modern Problems of Physics", Minsk 2014: 243-247.

[9] Mico V, Zalevsky Z, García-Martínez P, García J. Synthetic aperture superresolution with multiple off-axis holograms. JOSA A 2006; 23(12): 3162-3170. DOI: 10.1364/JOSAA.23.003162.

[10] Alexandrov SA, Hillman TR, Gutzler T, Sampson DD. Synthetic aperture Fourier holographic optical microscopy.

Phys Rev Lett 2006; 97: 168102. DOI: 10.1103/PhysRevLett.97.168102.
[11] Price JR, Bingham PR, Thomas CE. Improving resolution in microscopic holography by computationally fusing multiple, obliquely illuminated object waves in the Fourier domain. Appl Opt 2007; 46(6): 827-833. DOI: 10.1364/AO.46.000827.
[12] Chowdhury S, Izatt J. Structured illumination quantitative phase microscopy for enhanced resolution amplitude and phase imaging. Biomed Opt Express 2013; 4(10), 1795-1805. DOI: 10.1364/BOE.4.001795.
[13] Lehmann P, Niehues J, Tereschenko S. 3-D optical interference microscopy at the lateral resolution. International Journal of Optomechatronics 2014; 8(4): 231-241. DOI: 10.1080/15599612.2014.942924.
[14] Federici A, Dubois A. Full-field optical coherence microscopy with optimized ultrahigh spatial resolution. Opt Lett 2015; 40(22): 5347-5350. DOI: 10.1364/OL.40.005347.
[15] Safrani A, Abdulhalim I. Ultrahigh-resolution full-field optical coherence tomography using spatial coherence gating and quasi-monochromatic illumination. Opt Lett 2012; 37(4): 458-460. DOI: 10.1364/OL.37.000458.
[16] Grebenyuk AA, Ryabukho VP. Coherence effects of thick objects imaging in interference microscopy. Proc SPIE 2012; 8427: 84271M. DOI: 10.1117/12.922108.

Author's information

Anton Alexandrovich Grebenyuk, Candidate of Physical-Mathematical Sciences, has worked as a Docent at the Department of Optics and Biophotonics of Saratov State University and a Senior researcher at the Laboratory of Problems of Coherent-Optical Measurements in Precision Mechanics of the Institute of Precision Mechanics and Control of the Russian Academy of Sciences. Currently he is with the Christian Doppler Laboratory OPTRAMED, Center for Medical Physics and Biomedical Engineering, Medical University of Vienna. Research interests: optical coherence tomography/microscopy, quantitative phase microscopy. E-mail: *GrebenyukAA@yandex.ru* .

Vladimir Petrovich Ryabukho, Doctor of Physical-Mathematical Sciences, Professor, is a Professor at the Department of Optics and Biophotonics of Saratov State University and the Head of the Laboratory of Problems of Coherent-Optical Measurements in Precision Mechanics of the Institute of Precision Mechanics and Control of the Russian Academy of Sciences. Research interests: interferometry, holography, interference microscopy, coherence.

E-mail: *rvp-optics@yandex.ru* .

Code of State Categories Scientific and Technical Information (in Russian – GRNTI): 29.31.29.
Received December 1, 2017. The final version – February 7, 2018.